



Solar Corona Rotational Tomography: Diagnostics and Applications

Diego Lloveras¹, A. Vásquez², F. Nuevo², R. Frazin³

¹Grupo de estudios Heliofísicos de Mendoza, U. de Mendoza, Arg. ([GEHME](#))

²Instituto de Astronomía y Física del Espacio (CONICET–UBA), Arg. ([IAAFE](#))

³Department of Climate and Space Sciences and Engineering, U. of Michigan, USA. ([CLASP](#))

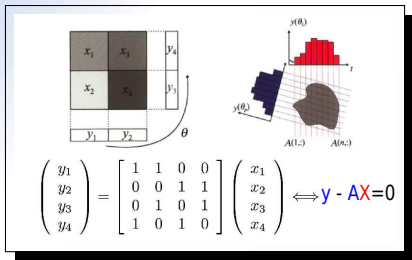
October 3, 2024

Tomography

Unknown: 3D distribution of a certain quantity x_i (e.g. N_e) for each cell volume i within an object (e.g. the solar corona), under optically thin regime (e.g. WL)

Knowns:

- **Intensity vector y_j :** measurement in each **pixel j** of each image of a time-series providing different view angles.
- **Projection matrix A_{ji} :** depending on the **geometry** (e.g. solar rotation, telescope orbit) and the involved **physical process** (e.g. Thomson scattering).



Tomographic reconstruction
C2-SRT (N_e) $2.5 - 6.5 R_\odot$

EUV-SRT
+ LDEM (N_e, T_e) $1.0 - 1.3 R_\odot$
=
DEM Tomography

- **Solar Rotational Tomography:** it is the solar rotation itself that provides the different viewing angles.

Solar Rotational Tomography (SRT)

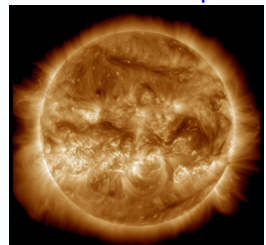
Radiation from the corona is caused by different phenomena

- K-Corona: Thomson scattering of photosphere WL → diagnostics of N_e
 - WL-SRT → 3D N_e
 - Altschuler & Perry (1972)
-
- E-Corona: Electronic decay of Iron ions emitting in EUV → diagnostics of N_e and T_e
 - EUV-SRT → 3D EUV emissivity → 3D DEM → 3D N_e and T_e
 - Frazin et al. (2009), Vasquez et al. (2009)

White light Coronagraph



EUV Telescope



The SRT Problem

The signal recorded by the j -th pixel is given by:

$$I_j = \int_{\text{LOS}_j} dl w(l) x(l) \rightarrow I = A \cdot X$$

I : Vector of J elements I_j , all pixels in all images.

A : Large sparse matrix of $J \times I$ elements $a_{j,i}$, purely geometrical.

X : Vector of I elements x_i , the discrete 3D distribution of the unknown:

WL-SRT

$$x(r) = N_e(r)$$

$$w(r) = S_{\text{Thomson}}(r)$$

EUV-SRT

$$x(r) = FBE_k(r) \equiv \int_0^{\infty} d\lambda \phi_k(\lambda) \eta(r, \lambda)$$

$$w(r) = 1$$

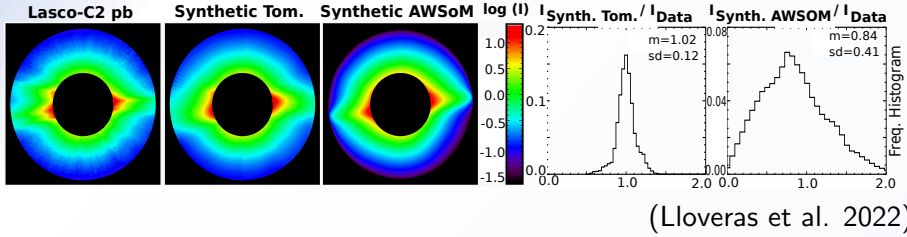
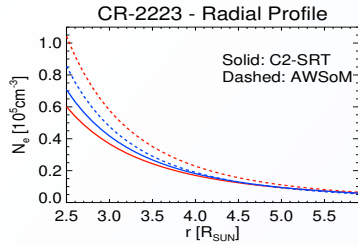
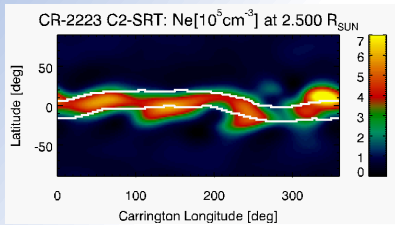
Solution: global optimization problem with cost function (of dimension- I):

$$f(X) = \|I - A \cdot X\|^2 + p \|R \cdot X\|^2$$

1st term: Difference between data and synthetic images.

2nd term: Regularization of the solution.

WL-SRT Validation of AWSOM



Data Image

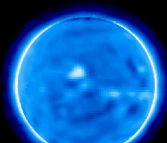
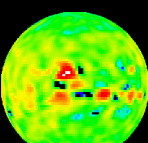
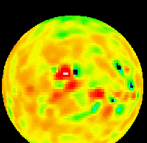
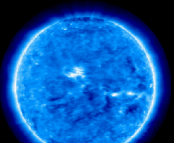
→

3D FBE

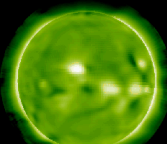
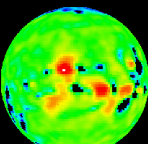
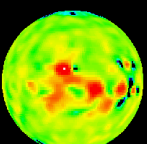
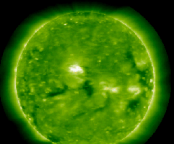
→

Synthetic Image

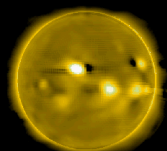
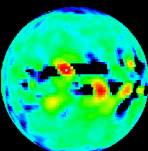
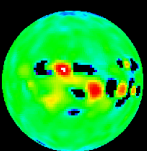
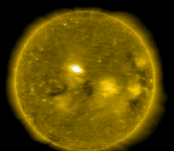
171 Å



195 Å



284 Å



$1.035 R_{\odot}$

$1.085 R_{\odot}$

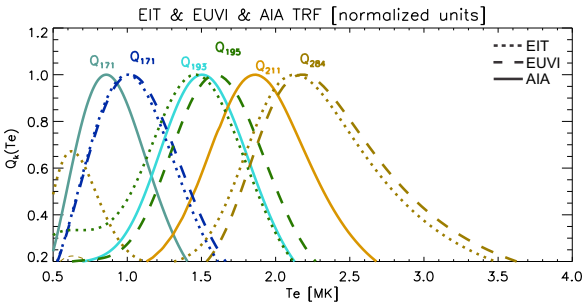
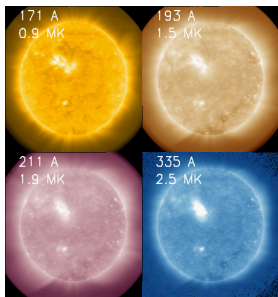
$1.135 R_{\odot}$

Vásquez et al. (2009)

Temperature Response of EUV Bands

Space telescopes have EUV detectors, whose filters mainly select Fe lines ($T_e \sim 0.5 - 2.5$ MK).

$$Q_k(T) \equiv \int d\lambda \phi_k(\lambda) \eta(N_{e0}, a_0, T; \lambda) / N_{e0}^2$$



- ϕ_k : Passband k
- $\eta(\lambda, T, N)$: Spectral emissivity model.
Chianti v10, Del Zanna et al. (2021)

Lloveras et al. (2018)

Local Differential Emission Measure (LDEM)

- For each band k we now know the $FBE_{k,i}$ at each tomographic voxel i .
- The FBEs can be re-written as: $FBE_{k,i} = \int dT Q_k(T) LDEM_i(T)$.
- Where the $LDEM_i(T)$ [$\text{cm}^{-6}\text{K}^{-1}$] of each voxel i is defined so that:

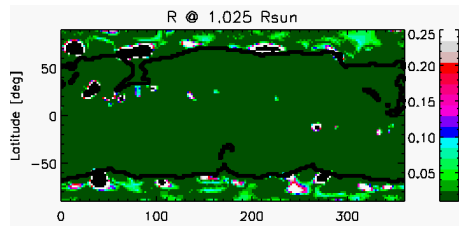
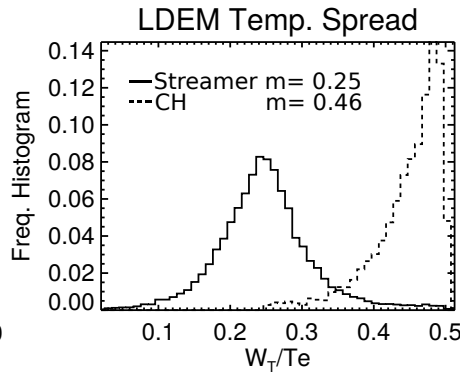
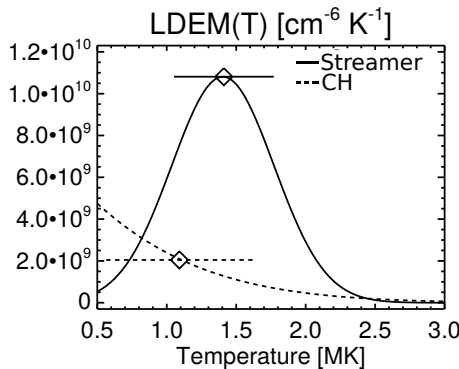
$$\begin{aligned} N_{m,i}^2 &= \langle N_e^2 \rangle_i = \int dT LDEM_i(T) \\ T_{m,i} &= \langle T_e \rangle_i = \frac{1}{\langle N_e^2 \rangle_i} \int dT T LDEM_i(T) \\ W_{T,i}^2 &= \frac{1}{\langle N_e^2 \rangle_i} \int_{T_{min}}^{T_{max}} dT LDEM_i(T) (T - \langle T_e \rangle_i)^2 \end{aligned}$$

- A parametric model for the LDEM is chose: $LDEM_i(T) = \mathcal{N}(T, \lambda_i = [A, T_0, \sigma_T])$
Nuevo et al. (2015)
- The following cost function is minimized in each cell:

$$\Phi(\lambda_i) = \sum_k |FBE_{k,i} - \int dT Q_k(T) \mathcal{N}(T, \lambda_i)|^2.$$

- Succes rate $R_i \equiv (1/K) \sum_k |1 - FBE_{k,i} / \int dT Q_k(T) \mathcal{N}(T, \lambda_i)|$

Typical LDEM

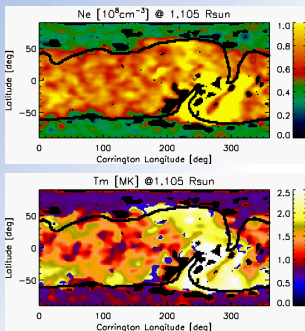


Lloveras et al. (2022)

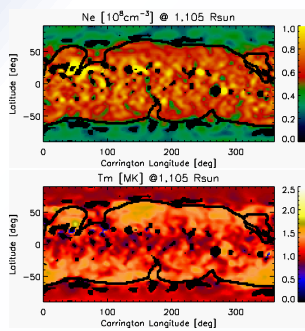
$$R \sim 1\% \text{ (Streamer)} \quad y \sim 10\% \text{ (CHs)}$$

EUV-SRT Comparative Solar Minima Study

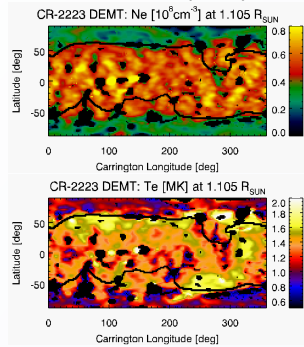
CR-1915 (EIT)



CR-2081 (EUVI)



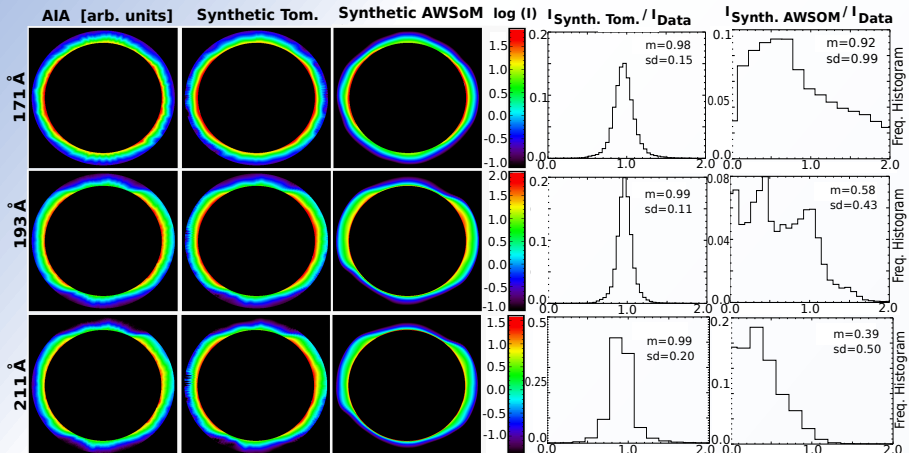
CR-2223 (AIA)



Lloveras et al. (2017,2020,2022)

- Azimuth symmetry
- Streamer(CHs) → higher(lower) density and temperature.
- Maximum gradients at O/C boundary

EUV Synthetic Images: EUV-SRT vs AWSOM



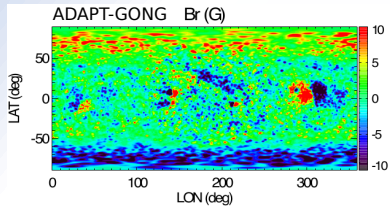
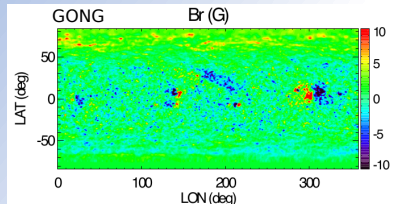
$$I_{\text{Synt}} \sim \int_{LoS} dI N_e^2 Q_k$$

- AWSOM O/C discrepancy due to lack of accuracy of boundary condition.

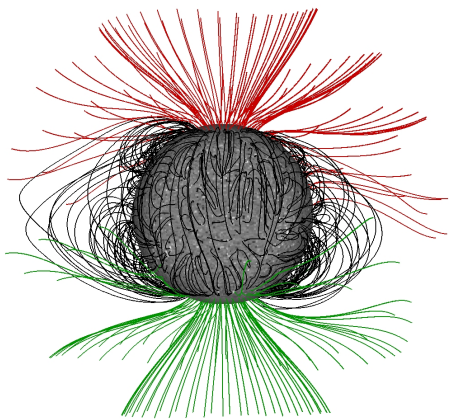
(Lloveras et al. 2022)

3D magnetic model

Sinoptic magnetogram (~ 28 days)

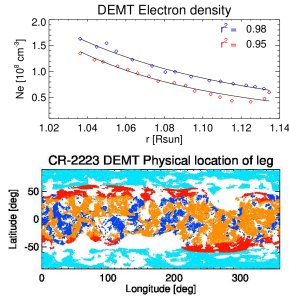
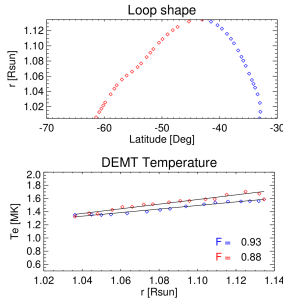
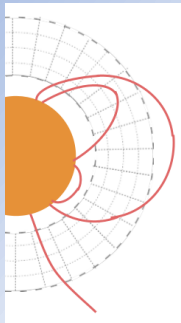


PFSS



- Assimilation Photospheric Flux Transport (ADAPT, Worden and Harvey, 2000): applies a magnetic flux transport model.

Tomographic Results along B-lines



Results along individual B-lines are characterized by parametric fits:

$$N_e^{(\text{EUV-SRT})} = N_0 \exp[-(h/\lambda_N)]$$

$$T_m = ar + b$$

and fitting parameters are analyzed statistically

UP ($a \equiv dT_e/dr > 0$)

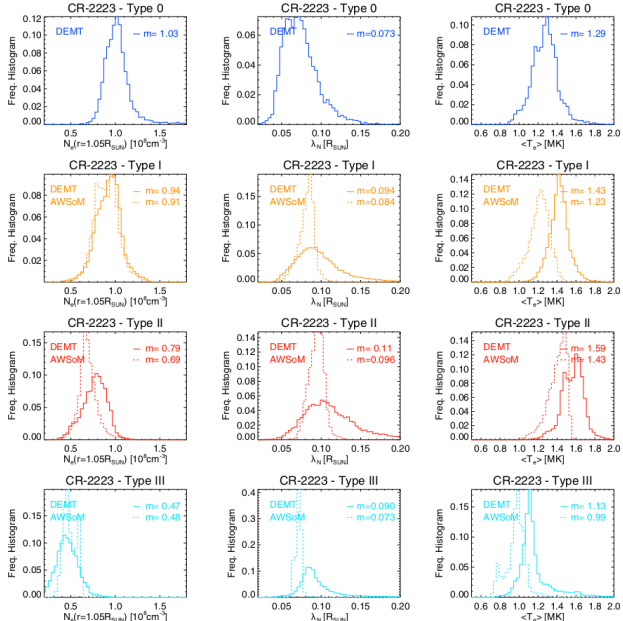
DOWN ($a \equiv dT_e/dr < 0$)

Table 1

Classification of Traced Magnetic Field Lines According to Their Geometry (Open/Closed), Size (Small/Large, Upon Apex Being Within/Outside the Range of Height of DEMT), Their Gradient of Temperature With Height (Up/Down, See Text), and the Footpoint Latitude θ_0

Type name	Open/Closed	Size	Up/Down	Footpoint latitude
0	Closed	Small	Down	$ \theta_0 < 50^\circ$
I	Closed	Small	Up	$ \theta_0 < 50^\circ$
II	Closed	Large	Up	$ \theta_0 > 40^\circ$
III	Open	Large	Up	$ \theta_0 > 60^\circ$

Results



Results DEMT

$$N_e^{(\text{DEMT})}(r) = N_0 \exp[-(h/\lambda_N) / (r/R_\odot)]$$
$$T_e^{(\text{DEMT})}(r) = T_0 + a h$$
$$h \equiv r - 1 R_\odot$$
$$\text{FOV} \sim 1.0 - 1.3 R_\odot$$

Table 2

Median Value (Indicated as "Md") of the Statistical Distribution of $N_{CB} \equiv N_e(r = 1.055 R_\odot)$, λ_N and $\langle T_e \rangle$ Shown in Figures 6 and 7

Type	Md(N_{CB}) [10^8 cm^{-3}]	Md(λ_N) [R_\odot]	Md($\langle T_e \rangle$) [MK]
CR-2219			
0	1.02	0.075	1.29
I	1.00 (-2%)	0.092 (-4%)	1.46 (-12%)
II	0.70 (+1%)	0.120 (-17%)	1.57 (-6%)
III	0.46 (+13%)	0.089 (-17%)	1.12 (-12%)
CR-2223			
0	1.03	0.073	1.29
I	0.94 (-3%)	0.094 (-11%)	1.43 (-14%)
II	0.79 (-13%)	0.110 (-13%)	1.59 (-10%)
III	0.47 (+2%)	0.090 (-19%)	1.13 (-12%)

Note. DEMT values are expressed in absolute terms, while AWSOM results are expressed relative to the corresponding DEMT value.

Lloveras et al. 2022

Results WL-SRT

$$N_e^{(\text{C2-SRT})}(r) = N_0 (r/2.5 R_\odot)^{-p}$$
$$\langle \lambda_N \rangle \equiv \left\langle \left| \frac{1}{N_e(r)} \frac{dN_e}{dr}(r) \right|^{-1} \right\rangle = \frac{4.25 R_\odot}{p}$$
$$\text{FOV} \sim 2.5 - 6.5 R_\odot$$

Table 3

Median Value (Indicated as "Md") of the Statistical Distribution of $N_e(r = 2.5 R_\odot)$ and $\langle \lambda_N \rangle$ Shown in Figures 11 and 12

Type	Md(N_e) [10^5 cm^{-3}]	Md($\langle \lambda_N \rangle$) [R_\odot]
CR-2219		
NH	0.72 (+40%)	1.43 (-10%)
SH	0.56 (+75%)	1.63 (-20%)
CR-2223		
NH	0.60 (+73%)	1.56 (-16%)
SH	0.70 (+21%)	1.45 (-9%)

Note. NH, northern hemisphere; SH, southern hemisphere. C2-SRT values are expressed in absolute terms, while AWSOM results are expressed relative to the corresponding C2-SRT value.

Lloveras et al. 2022